

Explainable and Hardware-Efficient Jamming Detection for 5G Networks Using the Convolutional Tsetlin Machine

Vojtech Halenka, Mohammadreza Amini *SMIEEE*, Per-Arne Andersen, Ole-Christoffer Granmo, and Burak Kantarci *SMIEEE*

Abstract—All applications in fifth-generation (5G) networks rely on stable radio-frequency (RF) environments to support mission-critical services in mobility, automation, and connected intelligence. Their exposure to intentional interference or low-power jamming threatens availability and reliability, especially when such attacks remain below link-layer observability. This paper investigates lightweight, explainable, and hardware-efficient jamming detection using the Convolutional Tsetlin Machine (CTM) operating directly on 5G Synchronization Signal Block (SSB) features. CTM formulates Boolean logic clauses over quantized inputs, enabling bit-level inference and deterministic deployment on FPGA fabrics. These properties make CTM well suited for real-time, resource-constrained edge environments anticipated in 5G. The proposed approach is experimentally validated on a real 5G testbed using over-the-air SSB data, emulating practical downlink conditions. We benchmark CTM against a convolutional neural network (CNN) baseline under identical preprocessing and training pipelines. On the real dataset, CTM achieves comparable detection performance (Accuracy 91.53 ± 1.01 vs. 96.83 ± 1.19 for CNN) while training $9.5\times$ faster and requiring $14\times$ less memory (45 MB vs. 624 MB). Furthermore, we outline a compact FPGA-oriented design for Zybo Z7 (Zynq-7000) and provide resource projections (not measured) under three deployment profiles optimized for latency, power, and accuracy trade-offs. The results show that the CTM provides a practical, interpretable, and resource-efficient alternative to conventional DNNs for RF-domain jamming detection, establishing it as a strong candidate for edge-deployed, low-latency, and security-critical 5G applications while laying the groundwork for B5G systems.

Index Terms—5G NR, Convolutional Tsetlin Machine, Interpretable Machine Learning, Jamming Detection, FPGA, Synchronization Signal Block (SSB), PSS/PBCH, Edge AI

I. INTRODUCTION

The increasing reliance of mission-critical services on the wireless medium inevitably exposes them to intentional radio-frequency (RF) interference (i.e., *jamming*), which can severely degrade network availability and service reliability. Traditional link-layer monitoring and performance counters often fail to capture such attacks, particularly when jammers operate at low power levels or exploit dynamic and fast-fading channel conditions to remain undetected [1]–[3].

V. Halenka, P-A. Andersen and O-C. Granmo, are with the Center of Artificial Intelligence Research, University of Agder, Grimstad, Norway. Emails: {vojtech.halenka,per.andersen}@uia.no
M. Amini and B. Kantarci are with the School of Electrical Engineering and Computer Science, University of Ottawa, Ottawa, ON, Canada. Emails: {mamini6,burak.kantarci}@uottawa.ca

Despite the growing volume of jamming detection work, many state-of-the-art solutions depend on higher-layer KPIs or deep models whose memory footprint, training cost, and limited transparency hinder deployment on IoT edge platforms. At the same time, the 5G SSB and PSS offer a deterministic, frequently transmitted physical-layer anchor whose distortions can reveal interference even when link-layer counters remain inconclusive. Motivated by this, we formulate RF-domain jamming detection directly from over-the-air SSB features and adopt the CTM as a lightweight, logic-based alternative to conventional CNNs. By learning Boolean clauses over quantized time-frequency patterns, the proposed detector couples interpretability with an on-edge deployable model, enabling a practical accuracy-efficiency trade-off for security-critical 5G networks.

The contributions of this paper are as follows.

- 1) Develop a robust Convolutional Tsetlin Machine (CTM)-based jamming detection framework that operates directly on over-the-air 5G signal features, eliminating the need for higher-layer performance indicator checks. The proposed detector is fully explainable and hardware-efficient, making it well-suited for deployment on resource-constrained IoT platforms.
- 2) Benchmark CTM against a strong Convolutional Neural Network (CNN) baseline on the same features. While the CNN attains slightly higher accuracy, CTM trains an order of magnitude faster with a $\sim 14\times$ smaller memory footprint, making it appealing for frequent updates and embedded deployment.
- 3) Provide projections for Zybo Z7: Zynq-7000 (Z7) board based on prior CTM-on-field-programmable gate array (FPGA) reports, outlining three deployment profiles with a different focus (Power, Latency, Accuracy).

Our results complement and extend recent Synchronization Signal Block (SSB)-centered jamming studies [4]–[7], by showing that machine learning (ML) can approach CNN accuracy on the same RF-domain features while significantly reducing training cost and model size—an attractive trade-off where power, memory, and deterministic latency matter.

The remainder of this paper is organized as follows. Section III describes the system model and problem formulation, including the 5G New Radio (NR) SSB structure and jamming hypotheses. Section IV details the proposed CTM-based jamming detection framework, covering preprocessing, Booleanization, and model configuration, along with the CNN

baseline for comparison. Section V presents the experimental results and performance analysis. Finally, Section VI concludes the paper with a summary of findings and future research directions.

II. RELATED WORK

A substantial body of literature has investigated 5G jamming detection mechanisms across different protocol layers. At the physical layer, researchers have exploited variations in signal-level statistics to infer abnormal interference patterns. These include the error vector magnitude (EVM), Received Signal Strength Indicator (RSSI), and time–frequency spectrograms [8]–[11]. Complementary studies have analyzed the impact of jamming on the cell-search and synchronization process itself, using behavioral deviations as detection cues [12], [13]. In parallel, a growing trend in the literature focuses on data-driven detection, leveraging supervised and unsupervised learning methods such as Deep Neural Network (DNN)s, autoencoders, and attention-based models [14], [15]. These approaches often achieve excellent classification accuracy and robustness against complex interference conditions. However, their reliance on large-parameter models and high-cost training/inference pipelines significantly limits their feasibility for deployment in real-time, resource-constrained edge or vehicular platforms.

In the 5G NR air interface, the SSB represents the essential downlink structure that supports the earliest stages of cell search and initial access [16], [17]. Because of its deterministic form, well-defined periodicity, and fixed mapping to the time–frequency grid, the SSB not only plays a pivotal role in establishing connectivity but also becomes an attractive target. Even selective or low-power jammers can impair the correlation of the Primary Synchronization Signal (PSS) and Secondary Synchronization Signal (SSS) or corrupt the decoding of the Physical Broadcast Channel (PBCH). Such impairments can obstruct Physical Cell Identity (PCI) discovery or system information decoding while keeping the jammer’s activity stealthy and energy-efficient [3], [18], [19].

To overcome these limitations, several studies have introduced lightweight machine-learning frameworks specifically tailored for 5G jamming detection. For example, the works in [6], [7] proposed advanced detectors based on a Trust Evaluation Data Analysis (TEDA) module and a Neural Network (NN) Deep Transformer-Driven Deep Denoising Neural Network (DT-DDNN), respectively. Both methods demonstrated strong detection capability and low false-alarm rates even under challenging signal-to-jamming-plus-noise ratio (SJNR) regimes. Nonetheless, despite their algorithmic elegance, the hardware and computational demands of TEDA and DT-DDNN remain prohibitive for practical integration into compact or embedded platforms.

Motivated by these operational constraints, this work revisits SSB-domain jamming detection through the lens of *Tsetlin Machine (TM)s* and their convolutional extension, the *CTM* [20]–[22]. Inspired by the successful application in similar domain [23], [24], we adapt the TM to this use case. TMs constitute a symbolic learning paradigm that formulates

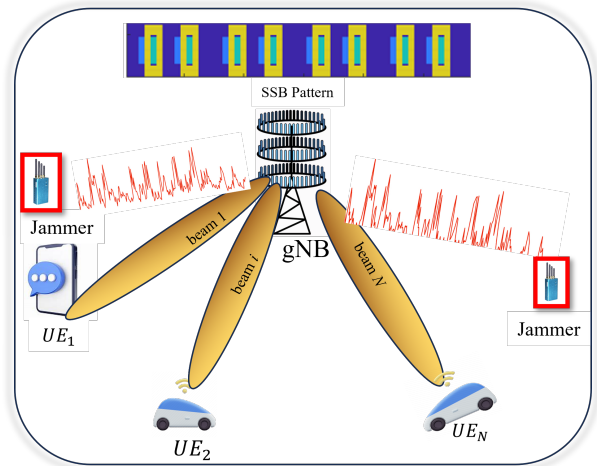


Fig. 1. Network Model in consideration

propositional logic clauses over Booleanized feature vectors using ensembles of learning automata (LAs). This results in models that are simultaneously interpretable, statistically efficient, and highly suitable for low-bit or integer-based implementation. Unlike conventional floating-point DNNs, TM and CTM inference operates via deterministic bit-wise logic, which naturally aligns with look-up table (LUT) and block RAM (BRAM) dominated FPGA architectures, as shown in [25], [26]. Consequently, they enable fully on-chip models characterized by low power consumption, predictable latency, and hardware-deterministic behavior. Moreover, recent FPGA-centric design flows—such as clause specialization, hierarchical clause sharing, and optimized bitstream synthesis—have further improved the area efficiency and scalability of large-clause TM deployments [27].

III. SYSTEM MODEL AND PROBLEM FORMULATION

Consider a 5G network where a next-generation NodeB (gNB) is located at the cell center, providing downlink services to multiple user equipments (UEs) distributed across the coverage area. In this environment, several malicious jammers attempt to disrupt the RF-domain transmissions, as depicted in Fig. 1. According to the SSB pattern specified in the 3GPP standard [16], the gNB periodically broadcasts synchronization signals across the network to enable UEs to perform cell search, timing acquisition, and initial access. In 5G NR, the PSS serves as the key element for initial cell search, sector identification, and time–frequency synchronization at the UE side. It constitutes the first orthogonal frequency-division multiplexing (OFDM) symbol of the SSB and is constructed from one of three predefined m -sequences $\Phi_{N_{ID}^{(2)}}(k)$, each corresponding to a sector identity $N_{ID}^{(2)} \in \{0, 1, 2\}$. These sequences are generated according to a linear feedback shift register (LFSR) recurrence relation that defines a length- $k_{pss} = 127$ pseudo-random binary sequence $s(i)$ as

$$s(i+7) = (s(i+4) + s(i)) \bmod 2$$

$$[s(6) \ s(5) \ s(4) \ s(3) \ s(2) \ s(1) \ s(0)] = [1 \ 1 \ 1 \ 0 \ 1 \ 1 \ 0] \quad (1)$$

where $s(i) \in \{0, 1\}$. The complex-valued PSS sequence in the frequency domain is then generated from the binary sequence as,

$$\begin{aligned} \Phi_{N_{ID}^{(2)},k} &= 1 - 2s(m) \\ m &= (k + 43 \times N_{ID}^{(2)}) \bmod k_{pss}, 0 \leq k < k_{pss} \end{aligned} \quad (2)$$

ensuring that each $\Phi_{N_{ID}^{(2)}}(k)$ is a circularly shifted version of the other two base sequences.

In the 5G resource grid, the PSS occupies the central 127 subcarriers of the first OFDM symbol ($l = 0$) within the SSB bandwidth, while the subcarriers outside this range are nulled to maintain spectral separation [16]. The PSS in frequency domain is written as

$$X_{l,k}^{ssb} = \begin{cases} \Phi_{N_{ID}^{(2)},k}, & k \in \{56, 57, \dots, 182\}, \\ 0, & \text{otherwise.} \end{cases} \quad (3)$$

After mapping the PSS to its respective subcarriers, the time-domain representation of the OFDM symbol is obtained through the inverse Fast Fourier Transform (FFT):

$$x_l^{ssb}(n) = \frac{1}{k_{ssb}} \sum_{k=0}^{k_{ssb}-1} X_{l,k}^{ssb} e^{j \frac{2\pi}{k_{ssb}} nk}. \quad (4)$$

The transmitted signal $x_l^{ssb}(n)$ then propagates through the wireless channel, where it experiences the channel impulse response $h(n)$ and additive thermal noise $z(n)$. Consequently, the received SSB at the user terminal can be modeled as

$$y_l^{ssb}(n) = x_l^{ssb}(n) * h(n) + z(n). \quad (5)$$

where N_{FFT} is the FFT length.

Since the PSS is transmitted in the first OFDM symbol ($l = 0$), the received PSS signal can be extracted directly from the first N_{FFT} samples of the received SSB as

$$y_{pss}(n) = y_l^{ssb}(n)|_{l=0}, \quad n \in \{0, \dots, N_{FFT} - 1\}. \quad (6)$$

The extracted PSS sequence $y_{pss}(n)$ serves as the basis for synchronization, channel estimation, and, in this work, jamming detection. The deterministic structure of the PSS, its fixed location in the resource grid, and its excellent auto-correlation properties make it an ideal reference for analyzing interference-induced distortions in the RF domain.

Under the null hypothesis H_0 , the received signal without jamming is,

$$H_0 : y_{pss}(n) = x(n) * h(n) + z(n) \quad (7)$$

Under the alternative hypothesis H_1 , where the jamming signal ($x_j(n)$) is present, the received PSS is

$$H_1 : y_{pss}(n) = x(n) * h(n) + z(n) + x_j(n) \quad (8)$$

The objective is to design a detection algorithm that discriminates between the two hypotheses and thus determines the presence or absence of a jamming attack. The receiver first extracts the PSS time–frequency representation from the recorded IQ samples by applying a short-time FFT and then constructs the input tensor for the CTM-based detector. This pipeline yields an explainable, hardware-efficient detector that remains effective against both constant and sophisticated jammers, including under high SJNR conditions.

IV. PROPOSED CTM-BASED JAMMER DETECTION

In this section, we present the proposed approach for jammer detection in 5G networks using the CTM.

A. Data Capturing and Preprocessing

The acquired over-the-air IQ samples undergo several preprocessing stages prior to feature extraction. First, raw base-band signals are captured by the receiver. To enable proper synchronization with the serving gNB, both carrier frequency offset (CFO) and time offset (TO) are estimated and compensated. Because the exact center frequency of the gNB is unknown, a blind search procedure is applied. The CFO is estimated by maximizing the correlation between the received and locally generated SSB waveforms as

$$\hat{f}_{\text{CFO}} = \arg \max_{f_i} \left[\sum_{\tau} y(\tau) e^{j2\pi \frac{f_i}{f_s} \tau} x_l^{ssb}(t - \tau) \Big|_{l=0} \right]. \quad (9)$$

Next, the Schmidl–Cox method [28] is adopted to determine the symbol-level timing offset by exploiting the cyclic prefix (CP) of the CP-OFDM waveform as,

$$\hat{t}_{off} = \arg \max_t M(t) = \frac{|P(t)|^2}{R(t)^2}, \quad (10)$$

in which $P(t)$ and $R(t)$ are presented as below:

$$P(t) = \sum_{m=0}^{L-1} y^*(t+m)y(t+m+L) \quad (11)$$

$$R(t) = \sum_{m=0}^{L-1} |y(t+m+L)|^2 \quad (12)$$

where L is CP length. After synchronization, the compensated waveform is aligned to the start of the SSB. The first OFDM symbol ($l = 0$) is extracted to isolate PSS for subsequent feature computation. This preprocessing chain ensures that the received signal is accurately frequency- and time-aligned with the gNB transmission, providing a clean input for the proposed for both the CNN and CTM-based jamming detector.

Next, we preprocess the data for TM-based classification. We tested several binarization techniques, resulting in sets of booleans, where each value represents a specific feature of the signal at a specific level, such as the presence or absence of a particular frequency or time pattern. This step is necessary for the TM, which operates on Boolean features.

B. CTM for Jamming Detection

Once the data is prepared and preprocessed, we apply the CTM [21] for the classification task, and compare with a conventional CNN.

In short, TM is a machine learning model based on propositional logic that uses a set of Tsetlin automata (TAs) to learn patterns in boolean data. As seen in Fig 2, the key advantages of TM arise from its native simplicity, and manifest as efficiency, transparency, and speed of classification of the model. For a thorough description of TM, see [20] and for CTM, see [21]. The CTM expands TM by processing the input data

in patches of predefined size, showing a convolutional view to the model. The processing includes attaching coordinates to each patch.

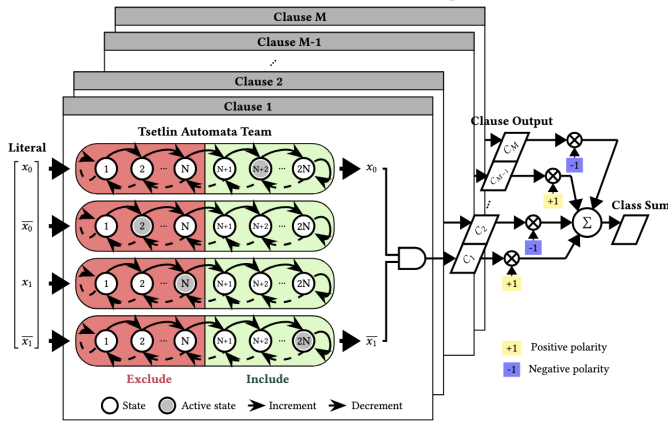


Fig. 2. The TM structure [29]

C. CTM Parameters

We use CTM with the configuration listed below. Values were tuned with Optuna [30] using 50 trials per preprocessing method on a validation subset and kept for all main results. The hyperparameter search space was

$$\begin{aligned} \text{number_of_clauses} &\in \{200\} \\ T &\in [50, 1000] \\ s &\in [1.0, 20.0] \\ \text{patch_dim} &\in \{5 \times 5, \dots, 10 \times 10\} \\ \text{max_included_literals} &\in [20, 64] \\ \text{epochs} &\in [3, 10] \end{aligned}$$

The best performing configuration on the validation set was with Enhanced Otsu method and the following parameters:

```
TMClassifier(number_of_clauses = 200,
             T = 477, s = 2.081,
             patch_dim = (10, 10),
             max_included_literals = 22)
```

D. CNN Baseline

For direct comparison with CTM, we trained a CNN, inspired by [6], on the same preprocessed spectrograms, reshaped to $(H, W, 1)$ with $H = W = 100$. The architecture comprises four convolutional blocks with progressively decreasing filter counts (256, 256, 128, 64), followed by two dense layers and a softmax head. Each convolutional block uses a 3×3 convolution with rectified linear unit (ReLU) activation, batch normalization, 2×2 max-pooling, and dropout (rate 0.25). The fully-connected stack consists of two dense layers with 512 and 256 neurons respectively, each followed by batch normalization and dropout (rate 0.5). The final layer is a 2-way softmax. We trained with Adam (learning rate 10^{-3}) and categorical cross-entropy loss, employing early stopping on validation accuracy with patience of 15 epochs.

a) *Model Complexity and Experimental Fairness:* The CNN baseline contains approximately 1.2 M trainable parameters and requires 45.3 M FLOPs per inference. To ensure fair comparison, both CTM and CNN were trained on identical splits of the dataset and preprocessed inputs. The CTM operates on binarized spectrograms (Enhanced Otsu thresholding), while the CNN uses normalized floating-point inputs. As an ablation study, we also evaluated the CNN on binarized inputs, which resulted in significant performance degradation (accuracy: 93.71 \rightarrow 74.69), confirming that CNNs benefit from continuous-valued features.

V. EXPERIMENTAL RESULTS

The raw baseband data within the 5G FR1 n71 band are captured using the ThinkRF RTSA R5500 spectrum analyzer. Controlled jamming is realized by injecting a synthesized interference waveform through a wireline RF combiner at the receiver front end, where it is superimposed on an over-the-air captured 5G signal. This experimental design allows precise control over jammer power and waveform characteristics while ensuring regulatory compliance by preventing over-the-air jamming transmissions. The acquired signals are recorded in CSV format via the PyRF4 API. Sampling is performed at a rate of 15.625 MHz with a carrier frequency of $f_c = 632$ MHz, corresponding to the Telus downlink center frequency. This configuration provides adequate spectral and temporal resolution for accurate synchronization and subsequent signal analysis.¹ The time-frequency features of the PSS, obtained via FFT, are then processed through the CTM pipeline. The complete set of experimental parameters is summarized in Table I. It is noted that the jammer signal, with multiple power levels as listed in Table I, is combined with the received 5G signal using an RF combiner.

TABLE I
SETUP AND ACQUISITION PARAMETERS FOR DATA COLLECTION.

Parameter	Value
Carrier Frequency (f_c)	632 MHz
Bandwidth	35 MHz
Sampling Rate	15.625 MHz
Antenna Type	Wideband omnidirectional
Duration per Capture	200 ms
FFT Size	1024
Jammer Transmit Gain	(-80 to -40) dB, step: 2 dB
Jammer Output Power	5 dBm
Receiver Gain	40 dB
CP Length	Normal

We evaluate CTM with various preprocessing methods against a CNN, on the same dataset with 5-fold cross-validation split. Both ran on the same hardware, Mac M1 Pro 16GB 2021. Table IV summarizes accuracy-oriented and model-oriented metrics. The CNN attains higher accuracies, while CTM offers markedly lower training cost and smaller memory footprint, making it attractive for rapid iteration and resource-constrained deployments (e.g., FPGA prototyping).

¹Since the n71 band is shared between two operators, the selected sampling rate satisfies the bandwidth requirements specified in [16].

a) *Booleanization*: We compared four binarization methods for CTM preprocessing: Enhanced Otsu (Otsu thresholding applied to both the original image and its 90°-rotated version, combined via logical OR), Paper Original (global standard-deviation-based denoising followed by mean-value thresholding), Multi-Level (Otsu thresholding at full 100×100 resolution and half 50×50 resolution, upsampled and combined via OR), and Adaptive Threshold (local Gaussian adaptive thresholding with block size 11×11). Enhanced Otsu achieved the best accuracy (91.75 ± 0.83) by capturing both horizontal and vertical edge patterns critical for jamming signal detection. See results of achieved accuracy scores using CTM in a 5-fold cross-validation study in Table II.

TABLE II
PREPROCESSING METHODS: 5-FOLD CROSS-VALIDATION ACCURACY WITH CTM BEST FOUND PARAMETERS

Preprocessing	Accuracy	s	T	patch	max_lit
Enhanced Otsu	91.53 ± 1.01	2.08	477	10×10	22
Paper Original	91.47 ± 1.06	3.64	326	10×10	28
Multi Level	90.88 ± 1.09	1.06	721	7×7	50
Adaptive Thresh	80.20 ± 1.64	1.78	192	9×9	30
CNN	96.83 ± 1.19	–	–	–	–

The CNN has shown only loss in performance when used with the same preprocessing techniques.

b) *Accuracy*: The CNN achieves higher scores than TM in almost all metrics, indicating stronger discriminative performance, as shown in Table III. However, there is a cost to that, in terms of memory and time.

TABLE III
ACCURACY AND COMPLEXITY METRICS OF CTM VS CNN

Model	Acc. [%]	Train. Time [s]	Infer. Time [s]	Mem. [MB]
CTM	91.96	44.4	2.5	45.2
CNN	96.81	3205.4	0.8	892.1

c) *Training cost*: TM trains about 9.6× faster (322 s vs. 3108 s) and sustains over an order of magnitude higher training throughput (4.97 vs. 0.41 samples/s). This gap makes TM appealing for rapid re-training when data distributions shift or when performing frequent on-device updates, with the hardware used in this study.

d) *Inference cost*: CNN inference is faster on this workload (5.11 s vs. 8.65 s total), yielding higher inference throughput (78.23 vs. 46.23 samples/s). If peak online throughput is the primary constraint, CNN currently holds an advantage.

e) *Memory footprint*: CTM uses ~14× less model memory (45.06 MB vs. 623.69 MB), which directly benefits embedded targets and eases model distribution/updates.

f) *Explainability*: In Fig. 3 and Fig. 4, we show the difference between features used for the classification of each model. The CNN seems to ignore lower frequency bands and focuses on specific parts of the spectrograph. Meanwhile, the CTM uses the lower frequency bands, in almost full time slot of the spectrograph to consider the sample as Pure. Same as in our preprocessed dataset, each pixel in the 100×100 spectrogram represents approximately 78.7 kHz of frequency

TABLE IV
CTM (INCL. PREPROCESSING) VS. CNN.

Metric	TM	CNN
Training Time (s)	321.69	3107.91
Inference Throughput (samples/s)	46.23	78.23
Model Memory Usage (MB)	45.06	623.69

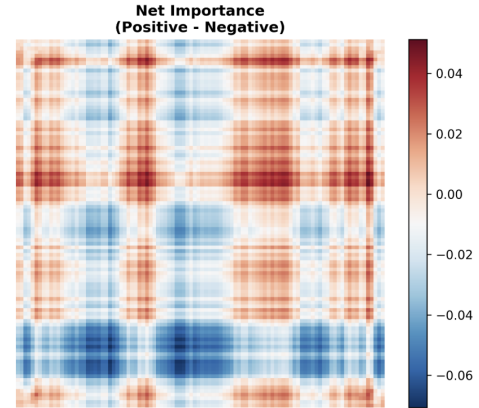


Fig. 3. Contributions of individual pixels, Red - Jamming, Blue - Pure, according to the trained CTM, using literal mentions count

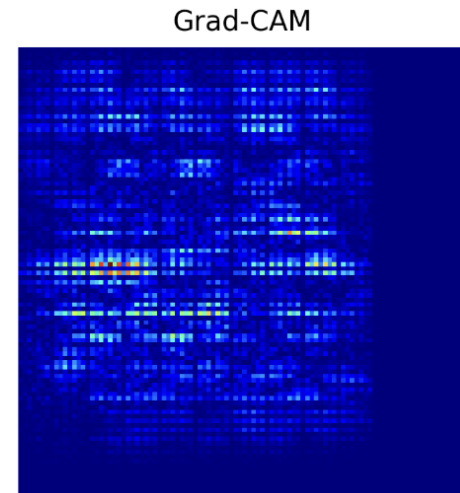


Fig. 4. Contributions of individual pixels, Red - Jamming, Blue - Pure, according to the trained CNN, using GradCAM

bandwidth from the original 15.625 MHz sampled signal. This can further be traced to the corresponding Resource Element.

g) *Takeaways*: CNN offers higher accuracy and faster inference, while TM is more training-efficient and compact. CNNs are a better fit for latency-critical tasks with high performance hardware; TMs fit constrained or frequently re-trained setups. Future work will explore lightweight CNNs and TM–CNN hybrids to combine strengths. Based on prior FPGA studies and logic-sharing methods (e.g. MATADOR), we estimate our CTM resource use on Z7 without new measurements. Assuming 30–60 LUTs per specialized clause with shared logic and RAM-stored TAs, Table V shows estimated deployment profiles.

TABLE V
PROJECTED CTM INFERENCE FOOTPRINTS ON Z7. LUTS USE A
30–60/CLAUSE ENVELOPE, 100 MHz, STRIDE = 1, AND 80 % EFFICIENCY.
NO NEW MEASUREMENTS; LITERATURE-BASED PROJECTION ONLY.

Profile	Clauses	LUTs	Samples/s
Power	256	~7.7k–15.4k	~1.0–2.5k
Latency	512	~15k–31k	~2.0–4.6k
Accuracy	800	~24k–48k	~1.1–2.5k

VI. CONCLUSION

This work introduced an explainable, hardware-efficient CTM as an edge deployable alternative to a CNN for jamming detection from 5G SSB features. If *maximizing detection accuracy and peak throughput* is the primary goal on general-purpose compute, the CNN is preferable (accuracy = 96.83 ± 1.19). If meeting tight edge constraints such as small memory, low power, predictable latency, and interpretability, is a priority, the CTM is advantageous: it maintained competitive performance (accuracy = 91.53 ± 1.01), trained $\sim 9.5\times$ faster, and required $\sim 14\times$ less model memory (45 MB vs. 624 MB). Literature-grounded FPGA projections further indicate that clause-specialized CTM designs fit within modest LUT envelopes on Z7 and can deliver kSamples/s-class effective throughput at 100 MHz, enabling fully on-chip, low-power deployment. In short: *choose CNN for absolute accuracy; choose CTM for explainable, resource-efficient edge inference.*

We are currently exploring hybrid CTM/CNN models and hardware-in-the-loop evaluations to optimize detection latency and resilience in dynamic RF environments, aiming to improve jamming defense in 5G and support progress toward B5G.

ACKNOWLEDGMENT

This work is supported in part by the Norwegian Directorate for Higher Education and Skills under Project Number UTF-2021/10133, and in part by the Natural Sciences and Engineering Research Council of Canada (NSERC) DISCOVERY and CREATE TRAVERSAL Programs.

REFERENCES

- [1] R. Khan, P. Kumar, D. N. K. Jayakody, and M. Liyanage, "A survey on security and privacy of 5g technologies: Potential solutions, recent advancements, and future directions," *IEEE Communications Surveys and Tutorials*, vol. 22, no. 1, pp. 196–248, 2019.
- [2] H. Pirayesh and H. Zeng, "Jamming attacks and anti-jamming strategies in wireless networks: A comprehensive survey," *IEEE Communications Surveys and Tutorials*, vol. 24, no. 2, pp. 767–809, 2022.
- [3] M. Lichtman, R. Rao, V. Marojevic, J. H. Reed, and R. P. Jover, "5g nr jamming, spoofing, and sniffing: Threat assessment and mitigation," in *IEEE Intl Conf on Communications Workshops*, 2018, pp. 1–6.
- [4] M. E. Flores, D. D. Poisson, C. J. Stevens, A. V. Nieves, and A. M. Wyglinski, "Implementation and evaluation of a smart uplink jamming attack in a public 5g network," *IEEE Access*, vol. 11, pp. 140705–140719, 2023.
- [5] G. Asemian, M. Kulhandjian, M. Amini, B. Kantarci, C. D'Amours, and M. Erol-Kantarci, "The impact of mobility, beam sweeping and smart jammers on security vulnerabilities of 5g cells," *arXiv preprint arXiv:2411.05131*, 2024.
- [6] G. Asemian, M. Amini, B. Kantarci, and M. Erol-Kantarci, "Dt-ddnn: A physical layer security attack detector in 5g rf domain for cavs," *IEEE Transactions on Vehicular Technology*, pp. 1–14, 2025.

- [7] M. Amini, G. Asemian, B. Kantarci, C. Ellement, and M. Erol-Kantarci, "Deep fusion intelligence: Enhancing 5g security against over-the-air attacks," *IEEE Transactions on Machine Learning in Communications and Networking*, vol. PP, pp. 1–1, 01 2025.
- [8] Y. Arjoune and S. Faruque, "Real-time machine learning based on hoeffding decision trees for jamming detection in 5g new radio," in *IEEE International Conference on Big Data*, 2020, pp. 4988–4997.
- [9] C. Örnek and M. Kartal, "An efficient evm-based jamming detection in 5g networks," in *IEEE MENACOMM*, 2022, pp. 130–135.
- [10] L. Chiarello, P. Baracca, K. Upadhy, S. R. Khosravirad, and T. Wild, "Jamming detection with subcarrier blanking for 5g and beyond in industry 4.0 scenarios," in *IEEE PIMRC*, 2021, pp. 758–764.
- [11] Z. Feng and C. Hua, "Machine learning-based rf jamming detection in wireless networks," in *Intl. Conf. on Security of Smart Cities, Industrial Control System and Communications*, 2018, pp. 1–6.
- [12] F. Chen, X. Li, Y. Zhang, and Y. Jiang, "Design and implementation of initial cell search in 5g nr systems," *China Communications*, vol. 17, no. 5, pp. 38–49, 2020.
- [13] R. Tuninato, D. G. Riviello, R. Garello, B. Melis, and R. Fantini, "A comprehensive study on the synchronization procedure in 5g nr with 3gpp-compliant link-level simulator," *EURASIP Journal on Wireless Communications and Networking*, vol. 2023, no. 111, pp. 1–20, 2023.
- [14] S. Jere, Y. Wang, I. Aryendu, S. Dayekh, and L. Liu, "Bayesian inference-assisted machine learning for near real-time jamming detection and classification in 5g new radio (nr)," *IEEE Transactions on Wireless Communications*, 2023, early Access.
- [15] Y. Wang, S. Jere, S. Banerjee, L. Liu, S. Shetty, and S. Dayekh, "Anonymous jamming detection in 5g with bayesian network model based inference analysis," in *IEEE International Conference on High Performance Switching and Routing (HPSR)*, 2022, pp. 151–156.
- [16] 3GPP, "Nr; physical channels and modulation," 3rd Gen. Partnership Project (3GPP), Technical Spec. (TS) 38.211, 2023, v17.6.0, Oct. 2023.
- [17] Z. Lin, J. Li, Y. Zheng, N. V. Irukulapati, H. Wang, and H. Sahlin, "Ss/pbch block design in 5g new radio (nr)," in *IEEE GLOBECOM Workshops (GC Wkshps)*, 2018, pp. 1–6.
- [18] N. Ludant and G. Noubir, "Sigunder: A stealthy 5g low-power attack and defenses," in *ACM WiSec*, 2021, pp. 250–260.
- [19] S.-D. Wang, H.-M. Wang, W. Wang, and V. C. M. Leung, "Detecting intelligent jamming on physical broadcast channel in 5g nr," *IEEE Communications Letters*, vol. 27, no. 12, pp. 3196–3200, 2023.
- [20] O.-C. Granmo, "The tsetlin machine: A game theoretic bandit-driven approach to interpretable pattern recognition," *arXiv preprint arXiv:1804.01508*, 2018.
- [21] O.-C. Granmo, S. Glimsdal, L. Jiao, M. Goodwin, C. W. Omlin, and G. T. Berge, "The convolutional tsetlin machine," *arXiv preprint arXiv:1905.09688*, 2019.
- [22] K. D. Abeyrathna, O.-C. Granmo, and M. O. Tveit, "A weighted tsetlin machine for classification," *arXiv preprint arXiv:1909.07310*, 2019.
- [23] S. Jeeru and et al, "Mixtme: A mixture of convolutional tsetlin machine experts using diverse spectrogram visualizations for jamming signal classification," *IEEE Internet of Things Journal*, pp. 1–1, 2025.
- [24] S. Jeeru, L. Jiao, P.-A. Andersen, and O.-C. Granmo, "Interpretable rule-based architecture for gnss jamming signal classification," *IEEE Sensors Journal*, vol. 25, no. 10, pp. 17942–17959, 2025.
- [25] S. A. Tunheim, L. Jiao, R. Shafik, A. Yakovlev, and O.-C. Granmo, "Tsetlin machine-based image classification fpga accelerator with on-device training," *IEEE Transactions on Circuits and Systems I: Regular Papers*, vol. 72, no. 2, pp. 830–843, 2025.
- [26] S. A. Tunheim, Y. Zheng, L. Jiao, R. Shafik, A. Yakovlev, and O.-C. Granmo, "An all-digital 8.6-nj/frame 65-nm tsetlin machine image classification accelerator," *IEEE Transactions on Circuits and Systems I: Regular Papers*, pp. 1–14, 2025.
- [27] D. Rule, A. Rashid, C. Blum, O. H. Sørensen, A. M. T. Marinho, and O.-C. Granmo, "Matador: Clause specialization and logic sharing for fpga-accelerated tsetlin machines," in *Design, Automation and Test in Europe Conference (DATE)*, 2024.
- [28] T. M. Schmidl and D. C. Cox, "Robust frequency and timing synchronization for ofdm," *IEEE Transactions on Communications*, vol. 45, no. 12, pp. 1613–1621, 1997.
- [29] S. Duan, R. Shafik, and A. Yakovlev, "Ethereal: Energy-efficient and high-throughput inference using compressed tsetlin machine," 2025. [Online]. Available: <https://arxiv.org/abs/2502.05640>
- [30] T. Akiba, S. Sano, T. Yanase, T. Ohta, and M. Koyama, "Optuna: A next-generation hyperparameter optimization framework," in *Proceedings of the 25th ACM SIGKDD International Conference on Knowledge Discovery and Data Mining*, 2019, pp. 2623–2631.